

# Radio Jet-Ambient Medium Interactions on Parsec Scales in the Blazar 1055 + 018

Joanne M. Attridge,<sup>1</sup> David H. Roberts,<sup>2</sup> and John F. C. Wardle<sup>3</sup>

Department of Physics, MS-057, Brandeis University, Waltham, MA 02454

## ABSTRACT

As part of our study of the magnetic fields of AGN we have recently observed a large sample of blazars with the Very Long Baseline Array. Here we report the discovery of a striking two-component jet in the source 1055 + 018, consisting of an inner spine with a transverse magnetic field, and a fragmentary but distinct boundary layer with a longitudinal magnetic field. The polarization distribution in the spine strongly supports shocked-jet models while that in the boundary layer suggests interaction with the surrounding medium. This behavior suggests a new way to understand the differing polarization properties of strong- and weak-lined blazars.

*Subject headings:* jets — galaxies: magnetic fields — polarization — quasars: individual (1055+018)

## 1. Introduction

Early VLBI polarimetry at 5 GHz revealed surprising differences between strong-lined and weak-lined AGN (loosely, ‘quasars’ and ‘BL Lacertae objects’) (Cawthorne et al. 1993). Sources with prominent emission lines, such as the classic quasars 3C 273 and 3C 345, are found to have primarily longitudinal magnetic fields in their jets (‘ $B_{\parallel}$ ’), while in weak-lined sources, such as the BL Lacertae objects OJ 287 and BL Lac itself, the magnetic field is transverse to the jet axis (‘ $B_{\perp}$ ’). However, this distinction is not universal, and sources with  $B_{\parallel}$  further out in their jets can also display  $B_{\perp}$  closer to the core (Leppänen, Zensus, & Diamond 1995). In the shocked relativistic jet paradigm under which these facts are generally understood, knots with  $B_{\perp}$  are the result of transverse shocks that compress and partially order an initially tangled magnetic field

---

<sup>1</sup>Current address: MIT Haystack Observatory, Route 40, Westford, MA 01886-1299  
E-mail: jattridge@haystack.mit.edu

<sup>2</sup>Visiting Scientist, National Radio Astronomy Observatory, and Department of Astronomy and Jet Propulsion Laboratory, California Institute of Technology  
E-mail: dhr@vlbi.astro.brandeis.edu

<sup>3</sup>E-mail: jfcw@quasar.astro.brandeis.edu

(Hughes, Aller, & Aller 1985). Regions with  $B_{\parallel}$  are thought to arise from interactions between the jet and the ambient medium, in which shear of the jet flow stretches the magnetic field along the jet (Wardle et al. 1994), or where the jet fluid is compressed against its boundaries (Laing 1980).

However successful, this picture does not explain why sources with different optical characteristics exhibit different jet polarizations. In an attempt to better characterize the relationship between optical and radio properties of AGN, we have observed a sample of 45 blazars with the VLBA<sup>4</sup> at 5 GHz at several epochs (Attridge, Wardle, and Roberts, in preparation). Here we present images of 1055 + 018 (= 4C 01.28 = DA 293 = OL 093), a blazar with  $z = 0.889$  (Wills & Lynds 1978). At this redshift 1 mas corresponds to  $7.27h^{-1}$  pc, and a proper motion of 1 mas yr<sup>-1</sup> corresponds to an apparent transverse speed of  $\beta_{app} = 44.7h^{-1}$  ( $H_0 = 70h$  km s<sup>-1</sup> Mpc<sup>-1</sup>,  $q_0 = 0.05$ ). The rest-frame emission-line equivalent widths of this source (Baldwin, Wampler, & Gaskel 1989; Falomo, Scarpa, & Bersanelli 1994),  $W_{eq}(\text{C III] } \lambda 1909) \simeq 8 \text{ \AA}$ ,  $W_{eq}(\text{Mg II } \lambda 2800) \simeq 5\text{--}12 \text{ \AA}$ , lie near the boundary  $W_{eq} = 5 \text{ \AA}$  used by some authors to divide blazars into weak- and strong-lined categories (Morris et al. 1991).

## 2. Observations

Images of 1055 + 018 were made from data taken on 1997 January 24 (epoch 1997.07), using all ten antennas of the VLBA plus a single antenna from the VLA ('VLBA+Y1'). The data were recorded at 5 GHz ( $\lambda 6$  cm) with total bandwidth of 64 MHz, and processed on the VLBA correlator. Approximately 4 hr were spent on source, leading to a root-mean-square noise of  $\sim 75 \mu\text{Jy}$  per beam. Calibration and hybrid imaging were done using the NRAO *AIPS* and Caltech DIFMAP packages. In our notation the total intensity is  $I$ , and the linear polarization is represented by the complex quantity  $P = Q + iU = pe^{2i\chi} = mIe^{2i\chi}$ , where  $p = (Q^2 + U^2)^{1/2} = mI$  is the polarized intensity,  $m$  is the fractional linear polarization, and  $\chi$  is the position angle of the electric vector. The integrated rotation measure of 1055 + 018 is  $-45 \text{ rad m}^{-2}$  (Kim, Tribble, & Kronberg 1991), which we take to be Galactic. This amounts to  $\Delta\chi = 9^\circ$  at 5 GHz, and has been removed in determining the direction of the magnetic field. Any additional Faraday rotation in or near the jet must be unimportant at 5 GHz; otherwise we would not find the striking magnetic field configuration described below. Complete details of VLBI polarization calibration and imaging techniques may be found in Cotton(1993), Roberts, Wardle, & Brown (1994), and Aaron (1996).

---

<sup>4</sup>The National Radio Astronomy Observatory is a facility of the National Science Foundation, operated under a cooperative agreement by Associated Universities, Inc.

### 3. Results

In Fig. 1a we show the total intensity distribution of 1055 + 018. This naturally-weighted image has a dynamic range (peak brightness/off-source noise) of  $\sim 17,000:1$ . A typical core-jet source, 1055 + 018 contains a bright unresolved component to the east and a jet extending at least 35 mas to the west north-west. The jet is resolved transverse to its axis (deconvolved width  $\gtrsim 3$  mas), and broadens considerably beyond  $\sim 12$  mas from the core. The true nature of the jet is revealed by the linear polarization distribution shown in Fig. 1b (dynamic range  $\sim 1100:1$ ). There we plot contours of linearly polarized intensity  $p$  with ticks showing the orientation  $\theta = \chi + \frac{\pi}{2}$  of the jet magnetic field (assuming optically-thin synchrotron radiation). It is apparent that the jet consists of two distinct parts: (1) a spine lying along the jet axis and containing a series of knots in which the magnetic field is predominantly perpendicular to the axis, and (2) a fragmentary boundary layer in which the magnetic field is predominantly parallel to the axis. Fig. 2 superimposes the  $I$  and  $P$  distributions, and shows clearly that the  $B_{\parallel}$  regions lie on the outermost visible edges of the jet. A natural interpretation of this two-component structure is that (1) transverse shocks dominate within the jet spine, so the net field there is perpendicular to the jet axis, and (2) in the boundary layer the magnetic field is determined by the jet's interaction with the surrounding emission line gas, resulting in a longitudinal field. This configuration is reminiscent of the 'spine-shear layer' morphology seen in the kiloparsec-scale jets of sources such as 3C 31 (Laing 1996) and 3C 353 (Swain, Bridle, & Baum 1996). Apparently 1055 + 018 displays simultaneously the magnetic field configurations characteristic of both weak- and strong-lined blazars, and as such provides us with an opportunity to study both the shocked-jet paradigm and the relationship between magnetic field orientation and optical properties for blazars.

In Fig. 3 we show the fractional polarization of 1055 + 018. At the jet boundaries  $m$  is quite high, exceeding 40% in places, so the magnetic field is well ordered, both across the sky and along the line of sight. The peak polarization in the jet spine is only  $\sim 10\%$ , presumably due to a combination of partially-tangled magnetic field in the knots and beam dilution by the unshocked jet (Wardle et al. 1994). There may also be some cancellation by any part of the boundary layer that intersects the line of sight. The magnetic field in the jet spine is predominantly  $B_{\perp}$ , so the shocked jet model predicts the knots to be more highly polarized than the regions between them (Wardle et al. 1994). That this is so can be seen in Fig. 3, and provides strong support for this model.

### 4. Discussion

There are some difficulties with the interpretation of the outer jet in 1055 + 018 as a parsec-scale version of the sheaths seen on much larger scales, i.e., as the cylindrically-symmetric outer layer of a coaxial jet. First, why is the jet in 1055 + 018 so wide so close the core? Three possibilities suggest themselves: (a) the true core is east of the easternmost component in our

images, and invisible either because it points away from us or it is severely self-absorbed, (b) the jet initially expands very rapidly but is quickly collimated, perhaps by the same forces that create the boundary layer, or (c) the jet is initially pointing almost exactly at us, but bends away from the line of sight within the first  $\sim 0.5$  mas. Second, why are the jet boundaries visible on only one side of the jet at a time? Perhaps they do not form a complete ‘sheath,’ but are those parts of the surface of the jet where the interaction with the ambient medium is strongest, most likely at the outer edges of smooth bends or at places where the jet is deflected. The jet curves to the south within its first 10 mas, and then turns northward over the next 15 mas, which is consistent with this possibility.

On kiloparsec scales, 1055 + 018 is a Fanaroff-Riley Type II radio source, with hotspots almost due north and south of the core, and a prominent jet in position angle  $\sim 180^\circ$  connecting the southern hotspot to the core; there is no sign of a jet to the north (Murphy, Browne, & Perley 1993). This source is thus an example of significant misalignment ( $\sim 120^\circ$ ) of jet orientation between parsec and kiloparsec scales. From tapered versions of Fig. 1a and from 1.6 GHz VLBI (Romney et al. 1984; Bondi et al. 1996) there are suggestions that beyond  $\sim 35$  mas from the core the jet continues to bend to the north. It would appear that on larger scales, the jet must bend through a very large angle (in projection) in order to connect with the kiloparsec-scale jet to the south. An alternative possibility is that the parsec-scale jet continues to the north, and that the kiloparsec-scale jet to the south is fed by an as-yet unseen parsec-scale counterjet. This seems less likely, since it would require *intrinsic* bends in both jets of more than  $90^\circ$ , assuming that the visible parsec-scale jet is pointing nearly towards us. High dynamic range VLBA images at lower frequencies, with superior surface brightness sensitivity and wider fields of view, may enable us to locate the bends and determine if and how the parsec- and kiloparsec-scale jets are connected.

Using the image presented here and two VLBA snapshot images at epochs 1996.02 and 1996.96, we have determined preliminary proper motions for the three brightest jet spine components relative to the the eastern-most component (the model fits are shown in Table 1). Unfortunately, the time base is short. For components C1 and C2 we find upper limits in apparent speed of about  $5h^{-1}c$ . For component C3, which is closest to the core, we derive a provisional speed of  $v_{app} = (12 \pm 4.5)h^{-1}c$ . Since the jet spine in 1055 + 018 has bright, well-defined knots, it will be straightforward to obtain reliable apparent velocities and accelerations for all of the knots over the next few years. This will also enable us to determine the physical parameters of the shocks in the jet spine, and their evolution (Wardle et al. 1994). Equally interesting will be attempting to detect proper motions for the boundary layer features. If this proves possible, the result would be a direct measurement of shear in a parsec-scale relativistic jet.

Velocity gradients across kilo-parsec scale jets have been inferred from their polarimetric properties (Laing 1996; Swain et al. 1996). If similar gradients are common on parsec scales, they may provide a new way to understand the connection between the apparent magnetic field orientation in blazar jets and the equivalent width of their broad emission lines. We suggest that the spine and the sheath have significantly different Lorentz factors  $\gamma$ ,  $\gamma_{spine}$  and  $\gamma_{sheath}$ ,

respectively, with  $\gamma_{spine} > \gamma_{sheath}$ . The radiation from the faster moving spine is beamed into a cone of opening angle  $\sim 1/\gamma_{spine}$ , while that of the sheath is beamed into a wider cone of opening angle  $\sim 1/\gamma_{sheath}$ . At small angles to the line of sight,  $\theta < \theta_{crit}$ , the polarization image is dominated by the faster moving spine, with its predominantly transverse magnetic field. At  $\theta > \theta_{crit}$ , the polarization image is dominated by the sheath, with its longitudinal magnetic field. If we further assume that the optical continuum radiation is also beamed with a Lorentz factor  $\gamma_{opt} \geq \gamma_{spine}$ , then at small angles to the line of sight, the optical continuum is strongly Doppler boosted with respect to the line emission, and the object will be classified as a “weak-lined blazar.” At larger angles to the line of sight, the continuum will be far less prominent, and the object will be classified as a “broad-lined blazar” (Aaron 1996). Close to the core, where the sheath has not fully developed, transverse magnetic fields are likely to be observed in both classes of object (Leppänen et al. 1995).

We conclude that 1055 + 018 is a touchstone for a number of important topics in the physics of AGN. Through it we can study the formation of the jet-like structure both along and across the axis, including bending and collimation, the conversion of bulk energy to microscopic particle energy and radiation, and the formation, propagation, and decay of shocks.

Radio astronomy at Brandeis University is supported by the National Science Foundation. The National Radio Astronomy Observatory is a facility of the National Science Foundation, operated under a cooperative agreement by Associated Universities, Inc. We thank many colleagues for their questions and suggestions on this work. D.H.R. thanks M. Goss, M. Cohen, S. Kulkarni, and R. Preston for their hospitality.

Correspondence and requests for materials should be addressed to J.M.A. (jattridge@haystack.mit.edu).

## REFERENCES

Aaron, S.E. 1996, Ph. D. Thesis, Brandeis Univ.

Antonucci, R. 1993, *Ann. Rev. Astron. Astrophys.* 31, 473

Baldwin, J.A., Wampler, E.J. & Gaskel, C.M. 1989, *ApJ*, 338, 630

Bondi, M., et al. 1996, *A&A*, 308, 415

Cawthorne, T.V., Wardle, J.F.C., Roberts, D.H., & Gabuzda, D.C. 1993, *ApJ*, 416, 519

Cotton, W.D. 1993, *AJ*, 106, 1241

Falomo, R., Scarpa, R., & Bersanelli, M. 1994, *ApJS*, 93, 125

Hughes, P.A., Aller, H.D., & Aller, M.F. 1985, *ApJ*, 298, 301

Kim, K.T., Tribble, P.C. & Kronberg, P.P. 1991, *ApJ*, 379, 80

Laing, R. A. 1980, *MNRAS*, 193, 439

Laing, R.A. 1996, In *Energy Transport in Radio Galaxies and Quasars*, ed. Hardee, P.E., Bridle, A.H. & Zensus, J.A. (PASP Conf. Series, Vol. 100, Astronomical Society of the Pacific, San Francisco), p. 241

Leppänen, K.J., Zensus, J.A., & Diamond, P.J. 1995, *AJ*, 110, 2479

Morris, S.L., Stocke, J.T., Gioia, I.M., Schild, R.E., Wolter, A., Maccacaro, T., & Della Ceca, R. 1991, *ApJ*, 380, 49

Murphy, D., Browne, I., & Perley, R. 1993, *MNRAS*, 264, 298

Roberts, D.H., Wardle, J.F.C., & Brown, L.F. 1994, *ApJ*, 427, 718

Romney, J., et al. 1984, *A&A*, 135, 289

Swain, M.R., Bridle, A.H., & Baum, S.A. 1996, In *Energy Transport in Radio Galaxies and Quasars*, ed. Hardee, P.E., Bridle, A.H. & Zensus, J.A. (PASP Conf. Series, Vol. 100, Astronomical Society of the Pacific, San Francisco), p. 299

Wardle, J.F.C., Cawthorne, T.V., Roberts, D.H., & Brown, L.F. 1994, *ApJ*, 437, 122

Wills, D., & Lynds, R. 1978, *ApJS*, 36, 317

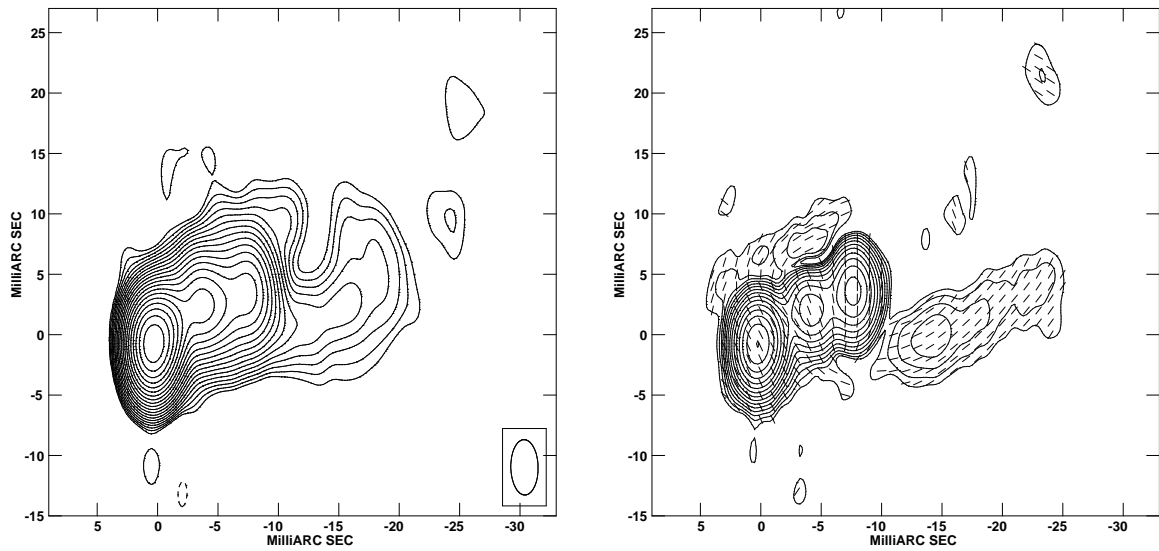


Fig. 1.— Naturally-weighted images of the blazar 1055 + 018, epoch 1997.07, made with the VLBA+Y1 at 5 GHz. (a) Total intensity distribution, with contours of  $I$  at  $-1.75, 1.75, 2.47, \dots$  [factors of  $\sqrt{2}$ ]  $\dots, 896$ , and  $1270$  mJy beam $^{-1}$ ; the peak is  $1720$  mJy beam $^{-1}$ , and the restoring beam shown in the lower right is  $4.6 \times 2.3$  mas at  $\phi = 1^\circ$ . (b) Linear polarization distribution, with contours of  $p$  at  $0.5, 0.707, \dots$  [factors of  $\sqrt{2}$ ]  $\dots, 45.3$ , and  $64$  mJy beam $^{-1}$ ; the peak is  $64.6$  mJy beam $^{-1}$ . The ticks show the orientation  $\theta = \chi + \frac{\pi}{2}$  of the magnetic field in the source. The restoring beam is the same as for  $I$ .

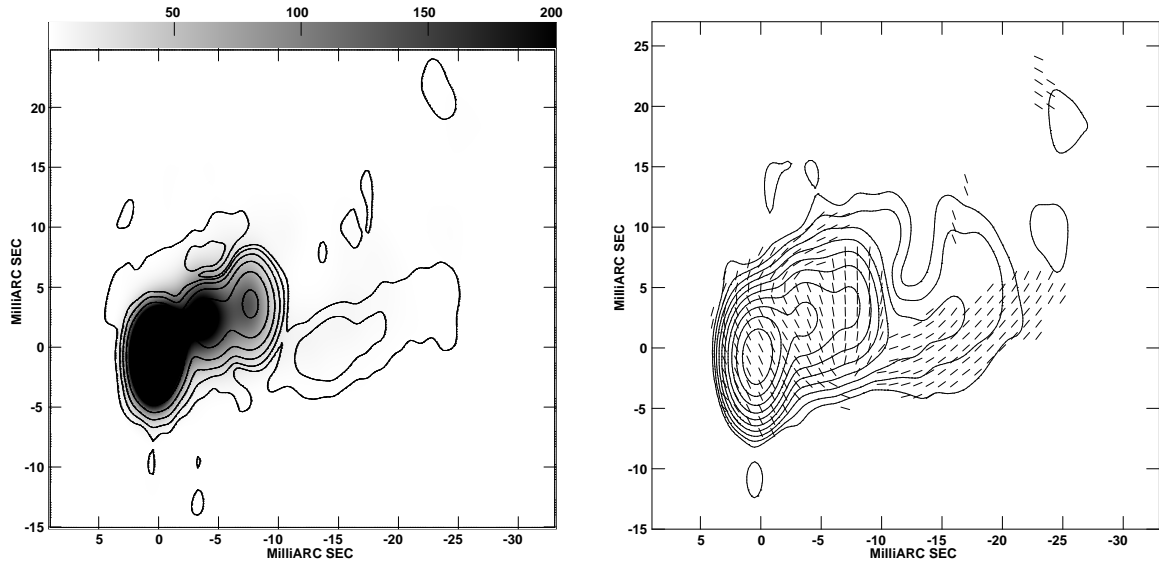


Fig. 2.— Superposition of the total intensity and linear polarization distributions of 1055 + 018, epoch 1997.07, made with the VLBA+Y1 at 5 GHz. (a) Every-other linearly polarized intensity contour from Fig. 1b over a grey scale image of the total intensity (the scale at the top is  $I$  in  $\text{mJy beam}^{-1}$ ); (b) every-other total intensity contour from Fig. 1a, plus tick marks showing the orientation  $\theta = \chi + \frac{\pi}{2}$  of the magnetic field in the source in those regions where the linearly polarized intensity exceeds 0.5  $\text{mJy beam}^{-1}$ , the lowest contour in (a).

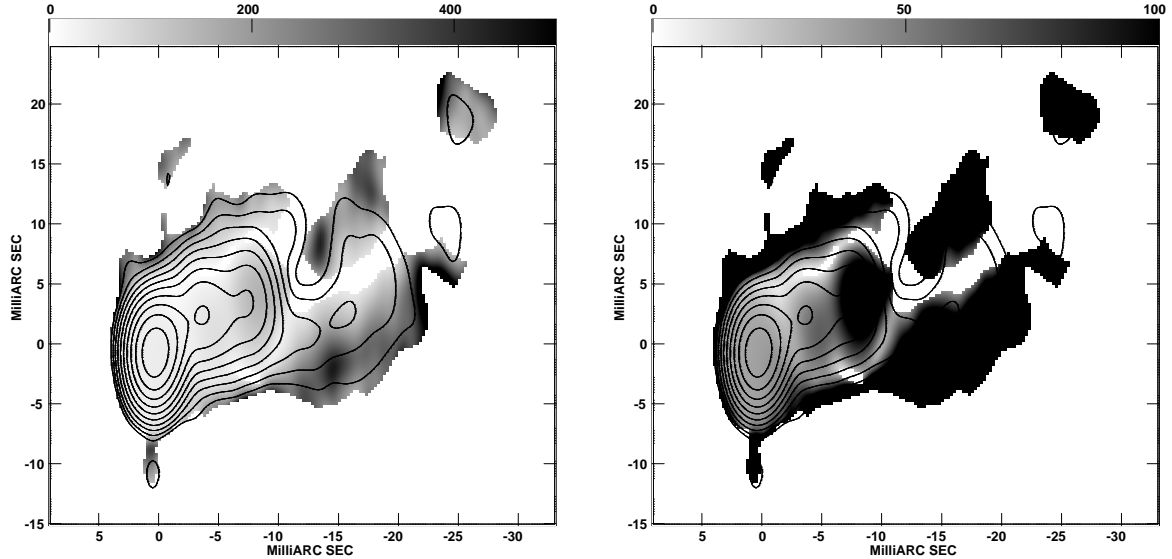


Fig. 3.— Superposition of every-other contour of total intensity  $I$  from Fig. 1a over grey scale for fractional linear polarization  $m$  in  $1055 + 018$  (the scales at top are  $1000 \times m$ ). (a) Polarization saturated at  $m = 0.5$  (showing details of the boundary layer), and (b) polarization saturated at  $m = 0.1$  (showing the spine).

Table 1. Jet Spine Components in 1055 + 018

Epoch	Component	<i>r</i> (mas)	$\theta$ (deg)	<i>I</i> (mJy)	<i>m</i> (%)	$\chi$ (deg)	maj. axis (mas)	min. axis (mas)	$\phi$ (deg)
(1)	(2)	(3)	(4)	(5)	(6)	(7)	(8)	(9)	(10)
1996.02	D	...	...	1190	2.8	-37.5	< 0.35	< 0.15	0.0
	C3	1.53	-48.6	431	2.9	-21.4	1.10	< 0.15	-60.1
	C2	5.26	-53.0	510	5.6	-71.8	3.38	2.76	-82.8
	C1	9.17	-61.2	176	11.3	74.6	3.85	1.84	3.0
1996.96	D	...	...	1350	3.1	-73.8	< 0.35	< 0.15	36.8
	C3	1.81	-46.5	394	5.0	-76.0	0.68	< 0.15	-37.7
	C2	5.30	-53.5	420	4.7	-72.8	2.70	2.52	-42.4
	C1	9.09	-61.3	198	11.8	78.8	3.82	1.73	2.1
1997.07	D	...	...	1590	3.5	-73.4	0.46	< 0.15	-35.0
	C3	1.79	-46.8	435	3.9	-72.4	0.79	0.19	-34.4
	C2	5.30	-52.2	469	3.9	-71.7	2.98	2.43	2.6
	C1	9.08	-61.3	276	10.4	78.1	4.51	2.17	2.6

Note. — (1) Epoch of observation, (2) component name, (3) distance from easternmost feature D, (4) PA of separation from D, (5) total intensity, (6) fractional linear polarization, (7) orientation of the linear polarization position angle, (8) major axis of the model component, (9) minor axis of the model component, and (10) orientation of the major axis.